ELF/VLF wave generation using simultaneous CW and modulated HF heating of the ionosphere

R. C. Moore[1] and D. Agrawal[1]

Received 2 July 2010; revised 11 January 2011; accepted 14 January 2011; published 19 April 2011.

[1] Experimental observations of ELF/VLF waves generated using the dual-beam heating capability of the High frequency Active Auroral Research Program (HAARP) HF transmitter in Gakona, Alaska, are compared with the predictions of an ionospheric HF heating model that accounts for the simultaneous propagation and absorption of multiple HF beams. The model output is used to assess three properties of the ELF/VLF waves observed on the ground: the ELF/VLF signal magnitude, the ELF/VLF harmonic ratio, and the ELF/VLF power law exponent. Ground-based experimental observations indicate that simultaneous heating of the ionosphere by a CW HF wave and a modulated HF wave generates significantly lower ELF/VLF magnitudes than during periods without CW heating, consistent with model predictions. Further modeling predictions demonstrate the sensitive dependence of ELF/VLF magnitude on the frequency and power of the CW signal. The ratio of ELF/VLF harmonic magnitudes is also shown to be a sensitive indicator of ionospheric modification, although it is somewhat less sensitive than the ELF/VLF magnitude. Last, the peak power level of the modulated HF beam was varied in order to assess the power dependence of ELF/VLF wave generation under both single- and dual-beam heating conditions. Experimental and theoretical results indicate that accurate evaluation of the ELF/VLF power law index requires high signal-to-noise ratio; it is thus a less sensitive indicator of ionospheric modification than either ELF/VLF magnitude or the ELF/VLF harmonic ratio.

Citation: Moore, R. C., and D. Agrawal (2011), ELF/VLF wave generation using simultaneous CW and modulated HF heating of the ionosphere, *J. Geophys. Res.*, *116*, A04217, doi:10.1029/2010JA015902.

1. Introduction

[2] It is by now well known that modulated HF heating of the lower ionosphere in the presence of auroral electrojet currents can be used as an effective means for generating electromagnetic waves with frequencies varying from less than several hertz to greater than several kilohertz (i.e., the ELF/VLF frequency band) [e.g., *Getmantsev et al.*, 1974; *Stubbe et al.*, 1982; *Barr et al.*, 1991; *Villaseñor et al.*, 1996; *Papadopoulos et al.*, 2003; *Moore et al.*, 2006; *Cohen et al.*, 2010]. Recent experimental and theoretical efforts have focused on methods to improve the efficiency of ELF/VLF wave generation. For instance, *Cohen et al.* [2010] explored the use of a creative technique that modulates the direction of the HF beam rather than the power of the HF beam to generate ELF/VLF waves, and *Milikh and Papadopoulos* [2007] theoretically analyzed the effect of long periods of CW heating prior to modulated heating. Recent hardware upgrades at the High frequency Active Auroral Research Program (HAARP) HF transmitter in Gakona, Alaska have provided an incredibly useful and versatile tool for probing and understanding the dynamics of high-power HF heating of the ionosphere. In particular, this paper will focus on the dual-beam transmission capability now available at HAARP to assess the veracity of a multiple-beam ionospheric heating model, noting that the manipulation of multiple HF beams may possibly lead to an improvement in ELF/VLF wave generation efficiency in the future.

[3] In this paper, we compare numerical modeling predictions with experimental observations in order to validate a multiple-beam ionospheric heating model. Each of the dual-beam transmissions in this experiment use the combination of a modulated HF wave and an unmodulated (CW) HF wave, including periods with the CW beam turned OFF (i.e., single-beam heating). We compare the relative ELF/VLF magnitudes during CW-ON and CW-OFF periods and show that the addition of a CW beam decreases the magnitude of the ELF/VLF wave observed on the ground. We explore this relationship theoretically as a function of the frequency and power of the CW beam. We identify the harmonic ratio as an additional sensitive indicator of ionospheric modification. Last, we demonstrate that although the magnitude of the ELF/VLF signal received on the ground decreases under CW-heated conditions, the rate of ELF/

[1]Department of Electrical and Computer Engineering, University of Florida, Gainesville, Florida, USA.

0148-0227/11/2010JA015902

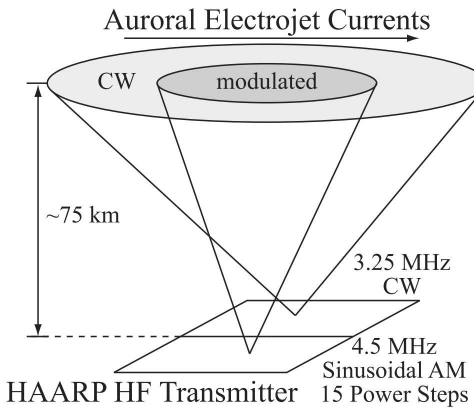

Figure 1. A cartoon diagram of the dual-beam HF heating experiment. The 3.25 MHz CW beam is broader than the 4.5 MHz modulated beam.

VLF magnitude change with the peak power of the modulated HF beam does not change significantly.

2. Description of the Experiment

[4] During a 30 min period between 0830 and 0900 UT on 2 August 2007, the 12 × 15 HAARP HF transmitter array was divided into two 6 × 15 subarrays, each with a peak power of 1800 kW. One subarray was used to generate ELF/VLF waves in the ionosphere by transmitting a sinusoidal amplitude modulated (at 1215 Hz and 2430 Hz) beam at 4.5 MHz (X mode polarization), stepping the peak HF power in 15 distinct log-based steps (from −12.5 dB to 0 dB with 1 s at each power level). Simultaneously, the second beam of the HAARP HF transmitter continually heated the same patch of ionosphere at peak power at 3.25 MHz (CW, X mode) for a period of 8 min. A lower HF frequency was selected for the CW beam so that the CW beam pattern would be broader than that of the modulated 4.5 MHz HF beam. The 8 min CW transmission block was followed by a 7 min period without CW heating (that is, the first beam continued to modulate at 4.5 MHz while the second beam was OFF). A cartoon depiction of the HF beam configuration can be seen in Figure 1, and a diagram of the modulation frequency and HF power format can be seen in Figure 2. The gains of the two subarrays depend on the frequencies transmitted. For the purposes of modeling, we have approximated the peak effective radiated power (ERP) levels (using 6 × 15 subarrays) to be 78.9 dBW at 3.25 MHz and 84.2 dBW at 4.5 MHz. The 15 min experiment was repeated twice during the 30 min window, and the K_P index was 2 at this time.

[5] ELF/VLF wave observations were performed at a ground-based receiver located at the HAARP observatory, approximately 1.5 km from the HF transmitter. The radial and azimuthal components of the magnetic field were monitored continually. The receiver is sensitive to magnetic fields with frequencies between ~500 Hz and ~45 kHz. Data were sampled at 100 kHz with 16-bit resolution. In post-processing, the narrowband ELF/VLF amplitudes and phases at the modulation frequencies and their harmonics were determined using 1 s long discrete Fourier transforms.

[6] The ELF/VLF receiver used at HAARP has been rigorously tested to determine whether the observed ELF/VLF signals could be artificially created by nonlinear demodulation of the HF wave arriving at the receiver. If this were the case, one would expect to observe nonlinear effects on other ELF and VLF signals recorded in the data at the time of transmission, and these effects are not observed. For instance, modulation sidebands are not observed on VLF transmitter signals (in the 20–25 kHz range), and natural VLF signals do not exhibit evidence of receiver saturation or other nonlinearities, despite the fact that these signals are typically many times stronger than the ELF/VLF signals generated by modulated heating of auroral electrojet currents. Additionally, direct measurements of common-mode and differential-mode signal coupling also suggest that the observed ELF/VLF signals are generated by modulated heating of the auroral electrojet currents, rather than by nonlinear demodulation of the HF wave in the receiver electronics. Injected common-mode signals at 1.6 MHz were reduced by 40 dB compared to signals at 1 kHz, and common-mode signals at higher frequencies were too small to be measured. Injected differential-mode signals measured at 1 MHz were reduced by 40 dB from the 1 kHz value. Higher-frequency differential-mode signals were also too small to measure accurately.

3. Experimental Observations

[7] Figure 3 shows the magnitude of the ELF/VLF signal observed at HAARP at 1215 Hz and 2430 Hz for the entire

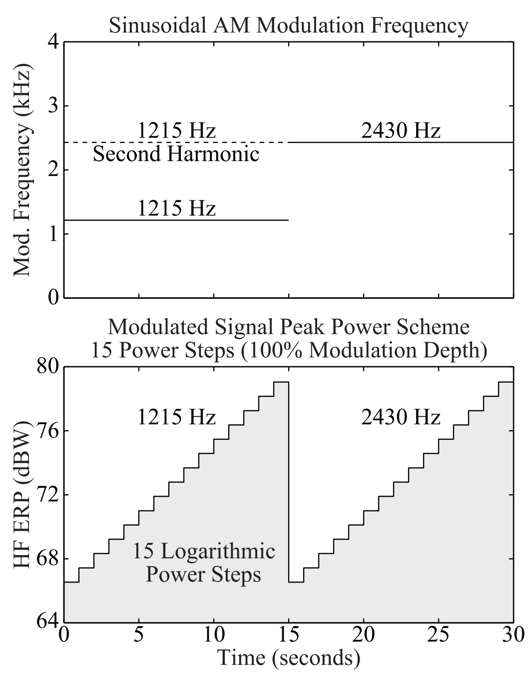

Figure 2. The transmission schedule for the 4.5 MHz modulated HF beam. (top) The modulation frequency (sinusoidal AM) as a function of time. (bottom) The peak power employed as a function of time. A modulation depth of 100% was used for all cases. Both panels share the same time axis. This 30 s schedule repeated continually for 30 min.

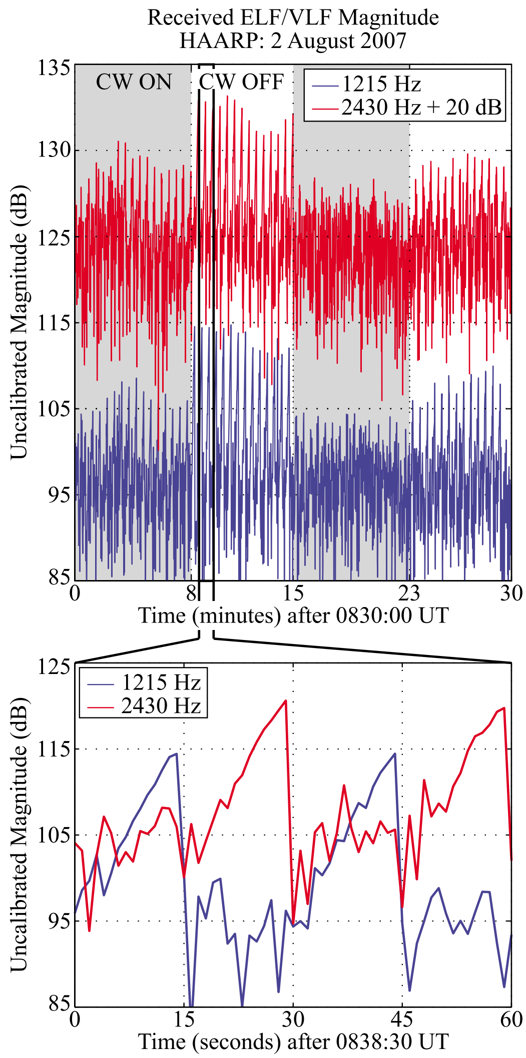

Figure 3. The magnitude of ELF/VLF signals observed at the ground-based receiver at HAARP. (top) All data for the 30 min duration of the experiment, with CW-ON and CW-OFF periods indicated with gray and white backgrounds, respectively. (bottom) Several examples of power step series observed during a CW-OFF block.

30 min duration of the experiment, with the CW-ON and CW-OFF periods indicated using a gray and white background, respectively. Good (>10 dB) signal-to-noise ratios (SNR) were observed during the first 15 min of the experiment. During the second 15 min period, the SNR decreased by approximately 5 dB. Figure 3 (bottom) shows several power step series during a CW-OFF period with a magnified time scale. From 0 to 15 s and from 30 to 45 s, the first and second harmonics (at 1215 Hz and 2430 Hz, respectively) clearly increase with transmitted power, which increases logarithmically over 15 s. From 15 to 30 s and from 45 to 60 s, a similar trend is observed, except that the 2430 Hz signal is the first harmonic (that is, the modulation frequency was 2430 Hz). When the second-to-first harmonic ratio is calculated later in section 3, we will divide the second harmonic magnitude at 2430 Hz(generated by the 1215 Hz transmission) by the first harmonic magnitude at 2430 Hz (generated by the 2430 Hz transmission), effectively canceling (to first order) the frequency-dependent effects of the Earth-ionosphere waveguide. The slopes of these traces (effectively on log-log scale) quantify the differential increase of ELF/VLF magnitude with peak modulated HF power.

[8] We will now discuss the observed ELF/VLF magnitudes in detail.

3.1. ELF/VLF Magnitude

[9] Figure 4 (left) shows the probability density functions (PDFs) for the SNR, the received ELF/VLF magnitude, and the ratio of ELF/VLF magnitudes recorded during CW-OFF periods to those recorded during CW-ON periods for observations at 1215 Hz. Figure 4(right) shows the same traces for observations at 2430 Hz. These PDFs are calculated using all available data points (including all power steps) in order to provide statistical significance. To calculate the SNR, noise levels are determined by extracting the ELF/VLF magnitudes at 1170 Hz (for comparison 1215 Hz) and at 2390 Hz (for comparison with 2430 Hz) as a function of time. At 1215 Hz, the SNR is on average 5.6 dB higher during CW-OFF periods than during CW-ON periods. At 2430 Hz, the SNR is4.4 dB higher during the CW-OFF periods than during the CW-ON periods. The results are similar for ELF/VLF magnitudes: at 1215 Hz, the ELF/VLF magnitude is on average 4.9 dB higher during CW-OFF periods, and at 2430 Hz, it is 4.1 dB higher. Figure 4 (bottom) shows the CW-OFF to CW-ON ELF/VLF magnitude ratio, calculated by dividing the observed magnitudes separated by 8 min in time. For reference, the noise has been processed in the same manner. As expected, the average

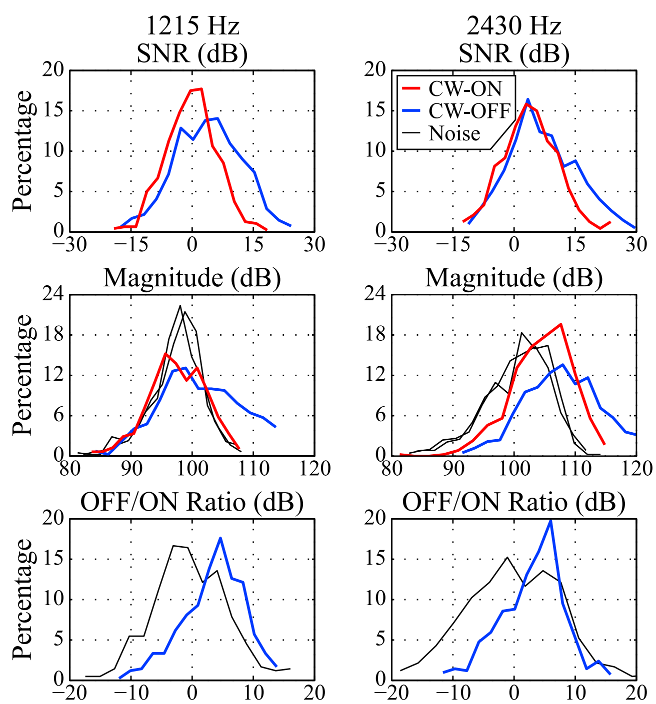

Figure 4. Statistical distributions (probability density functions): (left) 1215 Hz, (right) 2430 Hz, (top) SNR, (middle) magnitude, and (bottom) CW-ON to CW-OFF ratio calculated as described in the text.

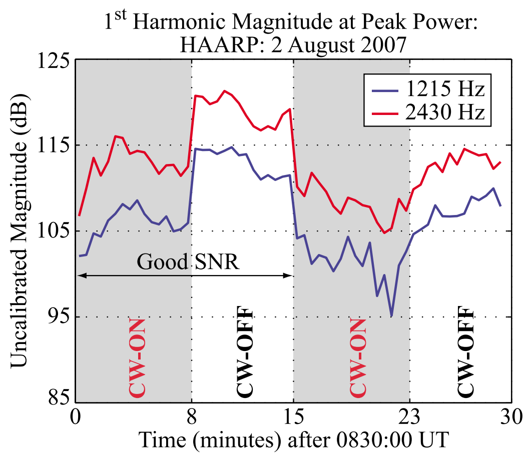

Figure 5. The magnitude of the first harmonic observed during only the peak power transmissions throughout the 30 min experiment. For each trace, there is one sample every 30 s.

results are similar: a 4.9 dB ratio is observed at 1215 Hz, and a 4.5 dB ratio is observed at 2430 Hz. The fact that these distributions are very similar to each other supports the statement that the ELF/VLF magnitude is significantly reduced by additional CW heating.

[10] In order to assess the effects of CW heating on the magnitude of the received ELF/VLF signal as a function of time, we select the magnitude of the first harmonic at the peak power transmission (i.e., the 15th power step). This selection supplies observations with the highest SNR. These magnitudes are available once every 30 s, and they are shown in Figure 5 for both 1215 Hz and 2430 Hz. The magnitudes exhibit a natural variation on the order of several dB over the 30 min experiment. This variation is likely dominated by the varying strength of the auroral electrojet currents, but also may be due to variations in electron density and electron temperature in the *D* region ionosphere. On the one hand, the variations in ionospheric parameters may be produced directly by HF heating; on the other hand they may also occur naturally, produced, for instance, by energetic electron precipitation or other natural phenomena. The observed change in ELF/VLF magnitude between CW-ON and CW-OFF periods, however, can be directly attributed to HF heating. At 1215 Hz and 2430 Hz, the magnitudes of the ELF/VLF signals increase by 8.6 and 8.1 dB, respectively, when the CW beam is turned off. The SNR at this point in time was 16.6 dB at1225 Hz and 22.2 dB at 2130 Hz. When the CW beam is turned on again 7 min later, the 1215 Hz and 2430 Hz magnitudes decrease by 7.4 and 9.1 dB, respectively. The SNR at this point in time was 16.7 dB at 1225 Hz and 17.8 dB at 2130 Hz. Observations during the second half of the experiment suffer from low SNR, although the data are not inconsistent with observations performed during the first 15 min of the experiment: the ELF/VLF field magnitudes are still higher during the CW-OFF period than during the CW-ON period.

[11] The large (7–9 dB) changes in ELF/VLF magnitude between CW-ON and CW-OFF periods indicate that the ELF/VLF magnitude may be used as a very sensitive indicator of ionospheric modification and that more detailed experiments may be performed. By alternating between CW-ON and CW-OFF periods once per second (or faster), the change in ELF/VLF magnitude may be tracked as a function of time, yielding insight into the variation of ionospheric parameters with much higher time resolution than available in the presented experiment. Additionally, the power and frequency of the CW signal may be varied, resulting in different changes in ELF/VLF magnitude between CW-ON and CW-OFF periods. Based on the large (7–9 dB) changes in ELF/VLF magnitude presented in this work, it is likely that these suggested experiments would yield measurable distinct changes ELF/VLF magnitude, and we directly assess this possibility in section 4.

[12] We now move on to discuss another sensitive experimental method to detect changes in ionospheric properties.

3.2. ELF/VLF Harmonic Ratio

[13] In this work, the ELF/VLF harmonic ratio is the ratio of the second harmonic magnitude to the first harmonic magnitude. For the presented experiment, ELF/VLF waves were generated using sinusoidal amplitude modulation, and the power envelope of the HF transmission thus consists of a first and second harmonic. If square wave amplitude modulation had been used, for instance, an equivalent measure would be the third harmonic to first harmonic ratio. In any case, the ratio of these two magnitudes generated at the same time essentially cancels strength of the auroral electrojet currents (to first order). Propagation within the Earth-ionosphere waveguide is strongly frequency dependent, however. In order to cancel the effects of the Earth-ionosphere waveguide (to first order), we require that the two magnitudes be measured at the same frequency. It is impossible to discern first and second harmonics generated at the same frequency at the same time, however. As a reasonable approximation, we generate the second harmonic at 2430 Hz using a 1215 Hz tone, and the first harmonic a short time later using a 2430 Hz tone. *Barr and Stubbe* [1993] used this method for evaluating harmonic ratios with great success to cancel (to first order) the frequency-dependent effects of the Earth-ionosphere waveguide.

[14] Because the SNR of the second harmonic is not particularly high throughout each of the 15 power steps, we use the second harmonic magnitude during only the peak power step (with ~5–10 dB SNR) to analyze the second-to-first harmonic ratio. The SNR of the first harmonic (at 2430 Hz) was ~20–25 dB during this time. Figure 6 shows the variation of the harmonic ratio over the course of the 30 min experiment. During the first CW-ON period, the harmonic ratio is essentially constant at −14.05 ± 0.4 dB. We attribute the two sharp, but temporary, deviations from this level to lightning-generated sferics coupling into the band rather than to changes in the properties of the ionosphere. When the CW beam turns off, however, the harmonic ratio immediately decreases by 3.75 dB to −17.8 ± 0.7 dB. During the CW-OFF period, the ratio again remains relatively constant, with two sharp deviations that likely result from lightning. During the second 15 min period of the experiment, observations suffer from low SNR. Despite this fact, some comparisons can be made. Upon turning the CW beam ON for the second time, the harmonic ratio immediately increases by 4.5 dB. During the second CW-ON period, the harmonic ratio fluctuates rapidly between −12 and

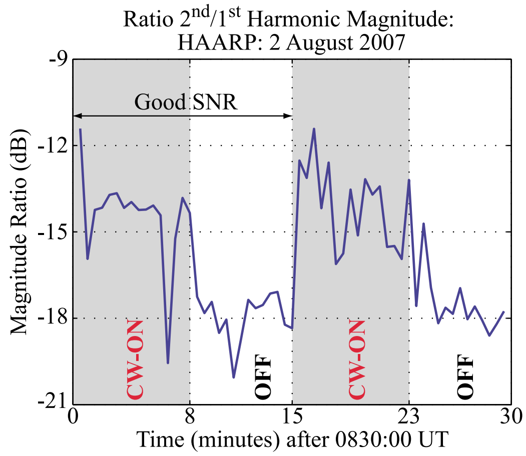

Figure 6. Ratio of the second harmonic magnitude to the first harmonic magnitude, calculated as discussed in the text, observed during only the peak power transmissions throughout the 30 min experiment. There is one sample every 30 s.

−15 dB due to low SNR, although we note that the −12 to −15 dB range includes the −14 dB level observed during the first CW-ON period. Approximately 1 min into the second CW-OFF period, the SNR increases somewhat, and the harmonic ratio remains close to −18 dB for the remainder of the period, similar to the first CW-OFF period.

[15] The assumption that the harmonic ratio is a sensitive indicator of ionospheric change under good SNR conditions will be evaluated numerically in section 4. Because the harmonic ratio is evaluated only once every 30 s, the immediacy of the −3.75 dB change and the +4.5 dB change at CW-ON/CW-OFF boundaries can only be stated with 30 s resolution. This may easily be improved during future experiments, however, by omitting the power stepping feature of the presented experiment.

[16] We will now discuss the observed dependence of ELF/VLF magnitude on HF power.

3.3. ELF/VLF Power Law Exponent

[17] In the early 1990s, *Papadopoulos et al.* [1990] and *Barr and Stubbe* [1991] suggested that the ELF/VLF magnitude depends on the peak input HF power as a power law with index n: $A_{\mathrm{ELF}} \propto P_{\mathrm{HF}}^{n}$. In this context, we will refer to the index n as the ELF/VLF Power Law Exponent (EPLE), which should in principle depend on the ambient properties of the D region ionosphere. For each power step series performed in our experiment, the EPLE is calculated using a weighted least squares fit to the observed ELF/VLF magnitude (in dB) as a function of HF power (in dB): $n = (P_{\mathrm{HF}}^{\mathrm{T}} W^{\mathrm{T}} W P_{\mathrm{HF}})^{-1}\ P_{\mathrm{HF}}^{\mathrm{T}} W^{\mathrm{T}} W A_{\mathrm{ELF}}$, with the weights of the matrix W determined by the SNR of the data points.

[18] Figure 7 shows the EPLE calculated for both 1215 Hz and 2430 Hz over the course of the experiment with 30 s resolution. During the first 15 min period, the EPLE measured at 1215 Hz is 0.63 ± 0.15 during the CW-ON period and 0.68 ± 0.11 during the CW-OFF period. No significant trends are observed during either the CW-ON or CW-OFF period, although they may be obscured by the noise. The EPLE exhibits a very subtle increase coincidentally with (within 30 s of) the change from CW-ON to CW-OFF. At 2430 Hz, the EPLE is measured to be 0.69 ± 0.16 during the CW-ON period and 0.78 ± 0.07 during the CW-OFF period. Again, no significant trends are observed during either period, although small trends may be obscured by the noise of the measurement. In this case, the EPLE appears to increase coincidentally (within 30 s) with the change from CW-ON to CW-OFF. During the second 15 min period, the SNR is too low for a reliable calculation of the EPLE. This effect is evident in the marked increase in measurement variability during the second 15 min period.

[19] The appearance of slight increases in EPLE at both 1215 Hz and 2430 Hz during CW-OFF periods may be misleading, however. Based on this data set, turning off the CW beam increases the EPLE by 0.05 ± 0.26 at 1215 Hz and by 0.09 ± 0.23 at 2430 Hz. The large uncertainties in the EPLE measurements indicate that it is not as well suited for evaluating changes in ionospheric properties as the ELF/VLF magnitude or the ELF/VLF harmonic ratio. Furthermore, it would be difficult to properly evaluate the EPLE with high time resolution. These conclusions will be evaluated in section 4.

[20] Having presented our experimental observations, we now turn our attention to the theoretical modeling of the dual-beam HF heating experiment.

4. Numerical Analysis

[21] The ELF/VLF wave generation model presented herein is implemented using two distinct calculations: (1) a

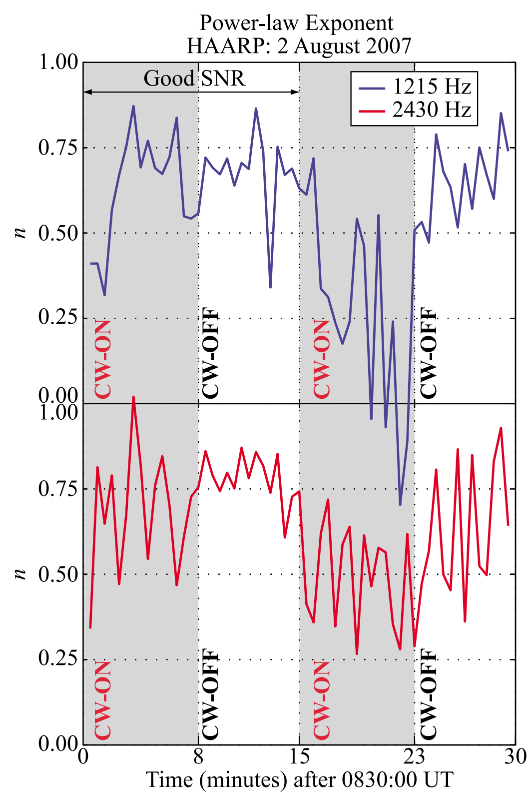

Figure 7. The power law exponent at 1215 and 2430 Hz for each power step series, calculated as discussed in the text. The two traces are separated for clarity. For each trace, there is one sample every 30 s.

dual-HF-beam ionospheric heating model is used to calculate the full time evolution of the ionospheric conductivity modulation as a function of space, and (2) a simple radiation model is employed to calculate the electromagnetic fields at the receiver. Here we discuss each of these calculations in turn, and then compare model predictions with the experimental results presented earlier in this paper.

4.1. Description of the Model

[22] The multiple HF beam ionospheric heating model is based on the single-beam HF heating model provided by *Moore* [2007]. The single-beam version has been used to successfully model ground-based ELF/VLF observations in a number of works [e.g., *Moore*, 2007; *Payne et al.*, 2007; *Lehtinen and Inan*, 2008]. Given a set of ionospheric profiles, including electron density and electron temperature height profiles, and given the parameters of the HF heating beam, such as the HF frequency, HF polarization, HF beam pattern, modulation frequency, and HF power, it predicts the time variation in electron temperature as a function of altitude within the highly collisional *D* region ionosphere. The model accounts for the self-absorption of the HF wave [e.g., *Tomko*, 1981] as well as for nonlinear electron energy losses [e.g., *Rodriguez*, 1994]. It neglects a number of ionospheric processes that are important at higher altitudes (but that are presumably less important in the *D* region), such as electron density changes that may result from long-term HF heating. The resulting variation in electron temperature is used to calculate the full time evolution of the so-called Hall, Pedersen, and Parallel conductivities, from which the amplitudes and phases of conductivity modulation at the modulation frequency and its harmonics are extracted.

[23] The model is ray based, meaning that a large number of rays are used to calculate the spatial extent of conductivity modulation. With a large enough number of runs, any HF radiation pattern may be modeled, including sidelobes, for instance. Typically, we reduce the total number of model evaluations by casting the system as cylindrically symmetric, although it is not necessary to do so, as has been demonstrated [*Payne et al.*, 2007]. In a cylindrically symmetric system, the Earth's magnetic field is oriented perpendicular to the Earth's surface at HAARP (~15° zenith angle in reality), and this is a good approximation for *D* region ohmic heating. The HAARP HF heating array is not cylindrically symmetric, however, particularly when 6 × 15 subarrays are utilized, as is the case in this paper. In order to approximate the system as cylindrically symmetric, the widths of the HF beam in the North–South and East–West directions are used to define a solid angle, and an effective cylindrically symmetric beam width is chosen such that it produces the same solid angle. This choice has the effect of producing approximately the same total volume of modulated currents.

[24] Here we describe the modifications made to the single-beam HF heating model to create a new multiple-beam heating model and evaluate the validity of the new assumptions. While the implemented analysis accounts for only two HF beams, the assumptions built in to this system are identical to those needed for a system consisting of more than two HF beams. This analysis, therefore, may be easily expanded to accommodate any larger number of HF beams.

[25] We begin with the well-known electron energy balance equation [e.g., *Huxley and Ratcliffe*, 1949; *Maslin*, 1974; *Stubbe and Kopka*, 1977; *Tomko et al.*, 1980; *Rietveld et al.*, 1986; *Rodriguez*, 1994]. For a single HF beam, the energy balance equation may be stated

$$\frac{3}{2} N_e \kappa_B \frac{dT_e}{dt} = 2k\chi(T_e)S - L(T_e, T_0) \tag{1}$$

where N_e is the altitude-dependent electron density, κ_B is Boltzmann's constant, T_e is the time-varying local electron temperature, k is the HF free space wave number, $\chi(T_e)$ is the temperature-dependent rate of absorption in the plasma (the imaginary part of the refractive index, n), S is the time-varying power density of the HF wave, and L is the sum total of all electron energy loss rates, which depend in general on both the ambient electron temperature T_0 and the time-varying electron temperature T_e. The model accounts for energy losses due to elastic collisions with [*Banks*, 1966], rotational excitation of [*Mentzoni and Row*, 1963; *Dalgarno et al.*, 1968], and vibrational excitation of [*Stubbe and Varnum*, 1972; *Prasad and Furman*, 1973] molecular nitrogen and oxygen. This equation neglects any time variation in the electron density (as mentioned above), and also neglects heat conduction as well as convection, as is typical for ELF/VLF wave generation models. Conduction and convection are typically neglected in *D* region modeling due to the fact that the characteristic time scales for electron heating and cooling are much smaller than parcel traversal time scales and heat conduction time scales. The long time scale (8 min) heating that is considered in this work may benefit by accounting for external drivers of convection, however. For instance, neutral wind speeds in the *D* region ionosphere can reach as high a 100 m/s [e.g., *Janches et al.*, 2009]. At this rate, a parcel of ionospheric plasma can traverse more than the entire width of the HF beam in an 8 min period. We expect that the primary effect of long-term convection is the limiting of electron density changes, however. Thus, for the purposes of this paper, convection is neglected.

[26] When accounting for two HF beams, the electron energy balance equation requires an additional term:

$$\frac{3}{2} N_e \kappa_B \frac{dT_e}{dt} = 2k_1\chi_1(T_e)S_1 + 2k_2\chi_2(T_e)S_2 - L(T_e, T_0) \tag{2}$$

where the subscripts, 1 and 2, identify quantities that depend on the HF beam. This additional term represents the energy absorbed by the local medium from a second HF wave. Similarly, if the number of HF beams is M, the electron energy balance equation may be written

$$\frac{3}{2} N_e \kappa_B \frac{dT_e}{dt} = \sum_{m}^{M} 2k_m\chi_m(T_e)S_m - L(T_e, T_0) \tag{3}$$

where the energy locally absorbed by the plasma from each of the M waves is contained within the summation term.

[27] The HF heating model simultaneously and self-consistently accounts for wave absorption as it calculates the trajectory of the HF ray paths (i.e., as it performs ray tracing). When accounting for multiple HF ray paths, it becomes clear that the frequency-dependent refraction and group velocity of the waves within the ionosphere will cause HF rays at different frequencies to become both spatially and

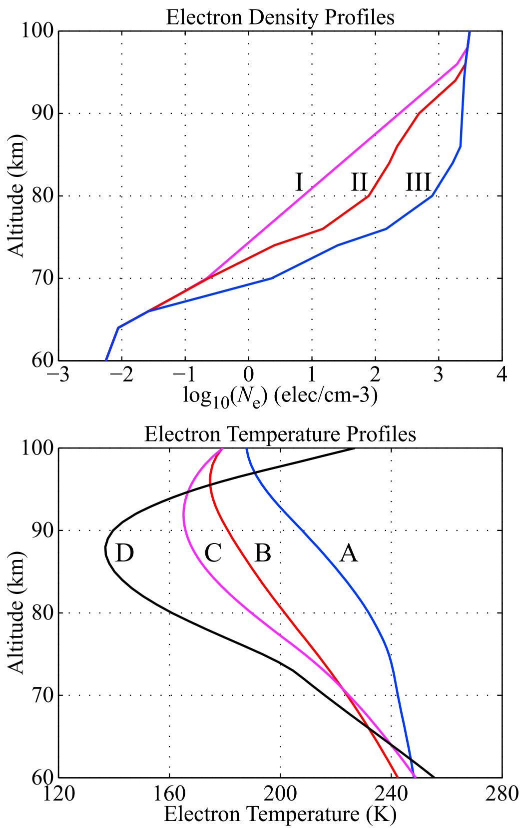

Figure 8. (top) Electron density profiles and (bottom) electron temperature profiles used in this work.

temporally separated. It is thus the case that any two HF waves at different frequencies that are transmitted at the same time and with the same initial trajectory will in general separate in both space and time as a function of propagation distance. We will assume that these effects are negligible for HF propagation below 100 km altitude.

[28] In order to evaluate this assumption, we use the twelve possible combinations of electron density and electron temperature profiles shown in Figure 8 and evaluate the temporal and spatial separation of HF beams at 3.25 and 4.5 MHz at an altitude of 100 km for initial HF ray angles varying from 0–30° zenith angle. The electron density profiles have been used in previous ELF/VLF wave generation analyses [e.g., *Moore et al.*, 2007] to represent tenuous (I) to dense (III) ionospheric conditions, and the electron temperature profiles are representative of a year-long survey of electron temperature profiles provided by the MSISE-90 Atmosphere Model hosted by NASA at http://ccmc.gsfc.nasa.gov/modelweb/. These same electron density and temperature profiles will be used throughout this work. Among all of the various combinations of electron density and electron temperature profiles, the maximum lateral spatial separation at 100 km altitude is calculated to be 72 meters, and the maximum temporal separation is calculated to be 0.8 μs. For the purposes of evaluating the generation of ELF/VLF conductivity modulation within the *D* region ionosphere, these separation values are not likely to be significant. For this reason, the multiple HF beam ionospheric heating model calculates the trajectory and timing of each ray path independently, but assumes the rays to be colocated for the purposes of evaluating ionospheric heating and HF wave absorption.

[29] It is notable that the dual-beam HF heating model does not automatically account for long-term changes in electron density. These changes are expected to occur on time scales much larger (by a factor >~1000) than the approximately millisecond timescales of ELF/VLF waves of importance to this work (1–3 kHz). Nevertheless, the long periods of CW heating in our experiment were designed in an attempt to induce these relatively slow electron density changes. In this paper, we evaluate the possibility of heater-induced electron density change using predictions calculated separately for the three electron density profiles shown in Figure 8, which represent electron density changes by a factor 1, 10, and 100 at 80 km altitude. For reference, the theoretical work presented by *Milikh and Papadopoulos* [2007] predicts an electron density change by a factor of ~2 under long-term HF heating conditions.

[30] In order to calculate the magnitude of the electromagnetic wave at the receiver, we first calculate the Hall, Pedersen, and Parallel currents in the ionosphere. The amplitudes and phases of the conductivity modulation calculated using the dual-beam HF heating model are interpolated onto a regular rectangular grid with 1 km spacing and multiplied by the electric field of the auroral electrojet, which is assumed to be 25 mV/m parallel to the ground, consistent with past theoretical work and experimental observations [e.g., *Banks and Doupnik*, 1975; *Stubbe and Kopka*, 1977; *Papadopoulos et al.*, 2003; *Payne*, 2007]. Because the experimental observations performed are all relative observations, the actual magnitude of the electrojet field strength does not matter in our case. We assume, however, that the spatial distribution of the electrojet field is uniform throughout the *D* region ionosphere.

[31] Using the Hall, Pedersen, and Parallel currents, we then calculate the electromagnetic field at the receiver using a formulation that accounts for a spatially distributed set of dipoles over a ground plane. Although this formulation does not account for the effects of the Earth-ionosphere waveguide, *Payne* [2007] demonstrated that for receiver locations within ~70 km of HAARP it closely matches a solution accounting for Earth-ionosphere waveguide effects. It should be noted, however, that the effects of the Earth-ionosphere waveguide are important. For instance, pronounced waveguide resonances at multiples of ~2 kHz have been observed in ELF/VLF amplitude data [e.g., *Stubbe et al.*, 1982; *Barr and Stubbe*, 1984; *Rietveld et al.*, 1989], and multiple ionospheric reflections have been directly observed during ELF/VLF pulsed heating experiments [e.g., *Papadopoulos et al.*, 2005]. It is very clearly the case that the Earth-ionosphere waveguide affects the amplitude and phase of the ELF/VLF signal received on the ground. The primary focus of this work therefore lies in evaluating the dual-beam heating portion of the model, with less of an emphasis placed upon evaluating the wave propagation model employed.

[32] As an illustrative example, Figure 9 shows altitude profiles of electron temperature and the amplitude of hall conductivity modulation. The maximum and minimum values of electron temperature over one steady state modulation period are shown for CW-ON and CW-OFF transmissions in

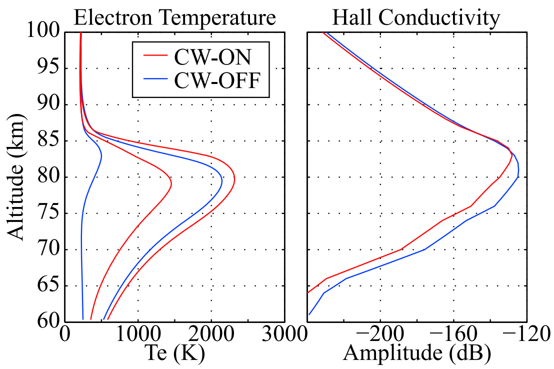

Figure 9. (left) Maximum and minimum electron temperatures achieved at sinusoidal steady state using electron density profile III and electron temperature profile D. CW-ON and CW-OFF periods are shown. (right) The amplitude of Hall conductivity modulation for CW-ON and CW-OFF.

Figure 9 (left). CW heating increases the maximum electron temperature achieved during the heating cycle, but increases the minimum electron temperature achieved to a greater extent. As a result, the modulation of the Hall conductivity is significantly reduced by CW heating (shown in Figure 9, right). The overall effect is a decrease in Hall conductivity modulation at lower altitudes, effectively increasing the altitude of the peak conductivity modulation from that for the CW-OFF case.

4.2. ELF/VLF Magnitude

[33] The magnitude of the predicted ELF/VLF B field on the ground is $\sqrt{B_H^2 + B_P^2}$, where K_H and B_P are the amplitudes of the B fields generated by the Hall and Pedersen currents, respectively. The assumption that the Earth's magnetic field is perpendicular to the ground means that the parallel conductivity is also perpendicular to the ground. As a result, the radial and azimuthal components of the direct path and ground-reflected B fields generated by the parallel conductivity cancel, and the parallel B field does not play a role in the predicted ELF/VLF magnitude. The quantity is conveniently independent of the orientations of the receiver antennas. It is useful to inspect the effect of CW heating on the generation of the Hall and Pedersen B fields independently, however. Figures 10 and 11 show the first harmonic amplitudes of the B fields generated by the Hall and Pedersen currents as a function of space within the lower ionosphere with a 1 km grid spacing. The colors represent the amplitude (in dB) of the ELF/VLF wave observed at the receiver and generated by a dipole at the plotted location. Figures 10 (left) and 11 (left) show the field amplitudes generated under modulated single-beam heating conditions

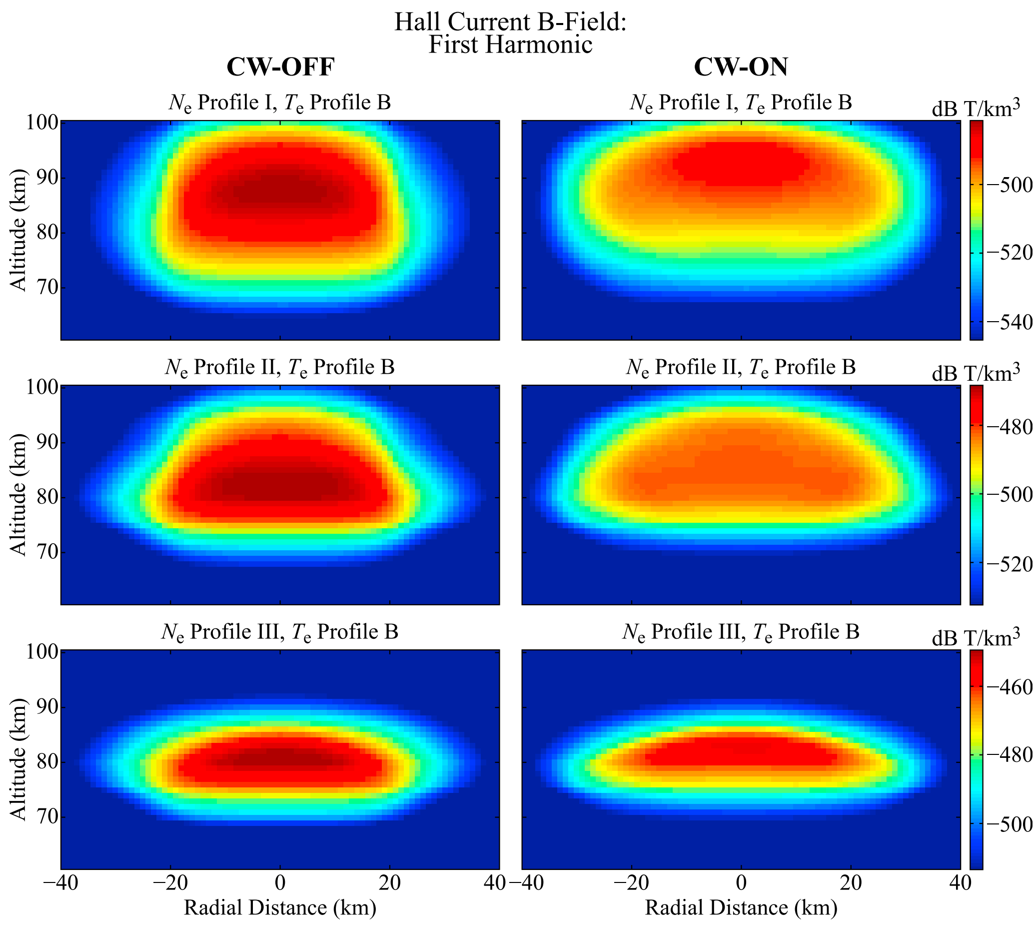

Figure 10. Numerical predictions. First harmonic (1215 Hz) Hall current B field amplitudes as a function of source location. CW-ON and CW-OFF periods are shown as a function of electron density profile.

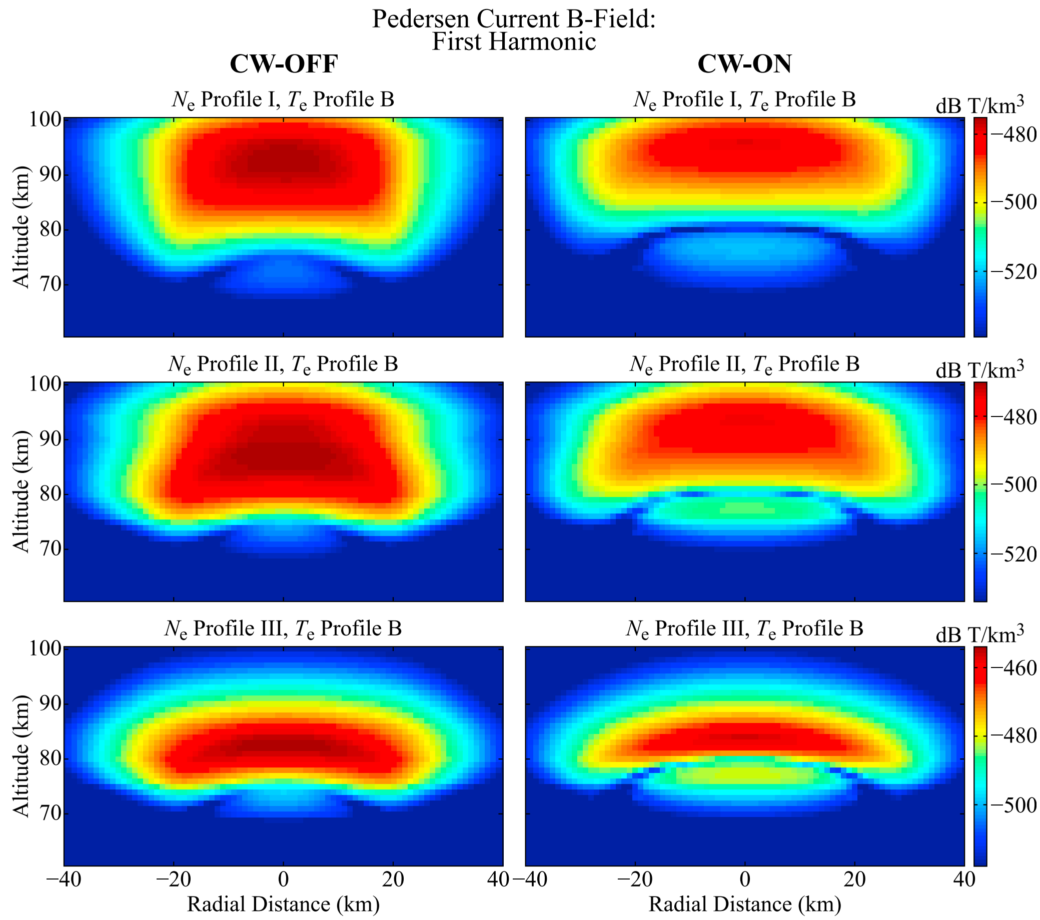

Figure 11. Numerical predictions. First harmonic (1215 Hz) Pedersen current B field amplitudes as a function of source location. CW-ON and CW-OFF periods are shown as a function of electron density profile.

(CW-OFF; sinusoidal AM at 4.5 MHz, X mode), and Figures 10 (right) and 11 (right) show the field amplitudes generated under dual-beam heating conditions (CW-ON at 3.25 MHz, X mode; sinusoidal AM at 4.5 MHz, X mode). Results are shown as a function of electron density, from Profile I (top) to Profile III (bottom), for a single electron temperature profile (Profile B). Figures depicting the dependence on the electron temperature profile (not shown) demonstrate essentially the same spatial distribution of fields shown here, although the absolute magnitudes are different. We note that the spatial distribution of the B fields shown is essentially cylindrically symmetric. In this case, the symmetry results from the fact that the receiver is located very close to (1.5 km from) the origin, in addition to the fact that we have forced cylindrical symmetry in the calculation of the conductivity modulation. For instance, plots calculated for a receiver distant from HAARP would show higher amplitudes in the direction of the receiver.

[34] Figures 10 and 11 demonstrate a pronounced dependence on the electron density profile. Under both CW-OFF and CW-ON conditions, the spatial distribution of both Hall and Pedersen currents becomes more compact in altitude as the electron density varies from Profile I to Profile III. Additionally, the altitude of the peak amplitude decreases significantly (by ~5 km per profile) and the peak amplitude itself increases sharply (by ~15 dB per profile) as the electron density varies from Profile I to Profile III. These effects may be due to an increase in electron density or may be due to an increase in the change in electron density with altitude, as the two are not differentiated in this work.

[35] The dependence on CW heating is also very clearly depicted in Figures 10 and 11. In all cases, the addition of a high-power CW heating beam "pushes" the wave generating currents upward and outward. The average altitude of wave generation increases, and the volume of radiating currents decreases at lower altitudes while at the same time increases at higher altitudes. The B field amplitudes are dramatically reduced at lower altitudes, but in some cases they increase slightly at higheraltitudes. In all cases, the peak amplitude decreases under CW-ON conditions. Figures 10 and 11 demonstrate that under a variety of electron density and electron temperature (not shown) conditions, additional CW heating will tend to reduce the magnitude of the ELF/VLF B field received on the ground.

[36] Figure 12, which shows the total B field magnitude received on the ground at 1215 and 2430 Hz as a function of electron density and electron temperature profile, quantifies this effect. At both modulation frequencies, the magnitude of the B field at the receiver increases with increasing (80 km) electron density at a rate of about 10 dB per

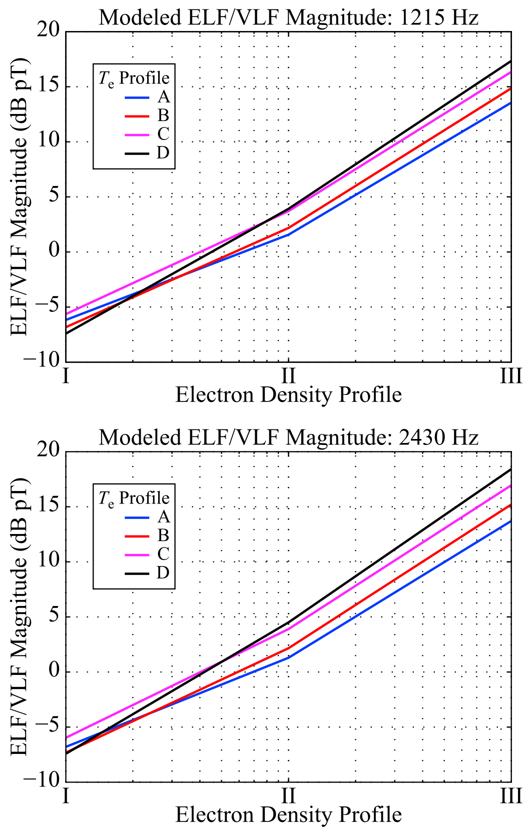

Figure 12. Numerical predictions. Total B field magnitude at the receiver as a function of electron density profile and electron temperature profile: (top) 1215 Hz and (bottom) 2430 Hz.

profile. Because the electron density increases by a factor of 10 between each profile, the x axis of these plots have an essentially logarithmic scale. Thus, a factor of 2 change in electron density at 80 km, as suggested by *Milikh and Papadopoulos* [2007], would produce ~3 dB increase in ELF/VLF magnitude on the ground by these estimates. This value is about half as large as the 7 dB increase in magnitude predicted by *Milikh and Papadopoulos* [2007]. The effect of ambient electron temperature is also important, as they may produce a 2–5 dB change in ELF/VLF magnitude. In most cases, the ELF/VLF B field magnitude increases with decreasing ambient electron temperature. The one exception is the combination of electron density Profile I with electron temperature Profile D. Together, these plots indicate that the ELF/VLF B field magnitude observed on the ground could be more effectively enhanced by the introduction of a chemical process that both increases the electron density and simultaneously decreases the electron temperature in the D region. The two effects are typically competing effects, however, as an increase in electron density also produces an increase in electron-neutral collision frequency.

[37] Figure 13 shows the change in ELF/VLF magnitude received on the ground during CW-ON and CW-OFF periods. Positive dB values on this plot indicate that the ELF/VLF magnitude is higher during CW-OFF periods than during CW-ON periods. We note that this model predicts that the B field on the ground is always higher during CW-OFF periods than during CW-ON periods, consistent with observations at these power levels. The observed 7–9 dB changes in ELF/VLF magnitude (shown in Figure 5) are slightly (~2 dB) higher than the predicted values shown in Figure 13. Nevertheless, the predicted values are reasonably close to the observed values. Considering that the additional CW heating tends to increase the altitude of the dominant ELF/VLF source currents, it may be the case that Earth-ionosphere waveguide effects, which depend upon both the altitude and frequency of the source and which are not accounted for in our wave propagation model, may account for the remaining residual (2 dB) between observed and modeled ELF/VLF magnitude.

[38] Considering the changes predicted for both modulation frequencies, the model predicts that the change in ELF/VLF magnitude on the ground is about 1 dB lower at 2430 Hz than at 1215 Hz. This was the case observed during the first CW-ON/CW-OFF transition, which is very encouraging, but it was not the case during the second CW-ON/CW-OFF transition, when the change in 2430 Hz magnitude was observed to change by 1 dB more than at 1215 Hz. Whether or not this is the typical observational case will not be resolved in this paper, but may easily be resolved by additional experimental studies. The frequency-dependent effects of the Earth-ionosphere waveguide may contribute to the discrepancy, which may also be affected by the assumption that the conductivity modulation is cylindrically symmetric. Despite these shortcomings, the model captures in a general sense the effects of simultaneous CW and modulated HF heating, in that it consistently predicts lower ELF/VLF magnitudes on the ground during CW-ON periods, and in that the predicted changes in magnitude are within ~2 dB of observations.

[39] The observed large 7–9 dB changes in ELF/VLF magnitude indicate that the ELF/VLF magnitude may be sensitive to the frequency and power of the CW beam. Figure 9 demonstrated that CW heating in addition to modulated HF heating increases the minimum electron temperature to a greater extent than the maximum electron temperature achieved at sinusoidal steady state. Thus, as the ERP of the CW beam increases from 0 to full power, we expect the minimum and maximum temperatures to increase from the

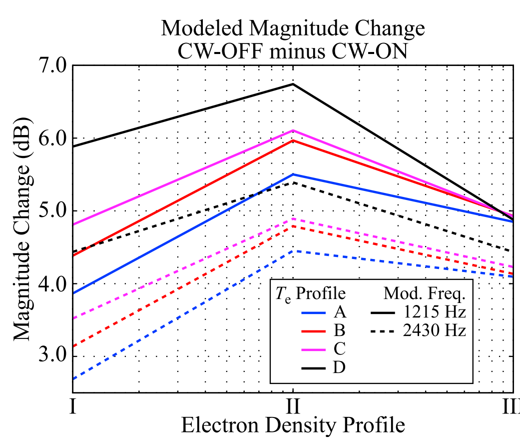

Figure 13. Numerical predictions. The change in total B field magnitude at the receiver from CW-OFF to CW-ON conditions.

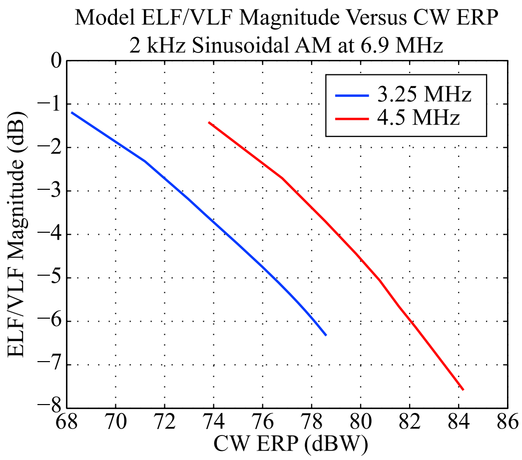

Figure 14. Numerical predictions. ELF/VLF amplitudes for modulated HF heating at 6.9 MHz and CW heating at 3.25 and 4.5 MHz (dB relative to CW-OFF) as a function of CW ERP.

CW-OFF traces to the CW-ON traces shown in Figure 9 (left). We also expect the amplitude of the Hall conductivity modulation (shown in Figure 9, right) to decrease gradually from the CW-OFF trace to the CW-ON trace, resulting in a gradual decrease in the ELF/VLF *B* field received on the ground. Figure 14 quantifies this effect and shows the model predictions for ELF/VLF magnitude as a function of the frequency and ERP of the CW beam. The ELF/VLF magnitudes shown are relative to the magnitude of the CW-OFF case. For Figure 14, the modulated HF frequency employed is 6.9 MHz, and the frequency of the CW beams are 3.25 and 4.5 MHz. For a given ERP, the lower CW frequency (3.25 MHz) suppresses the ELF/VLF magnitude to a greater extent than the higher CW frequency (4.5 MHz). At both CW frequencies, an increase in ERP further suppresses the ELF/VLF magnitude with nearly a power law relationship, and the power law exponents are only slightly different.

[40] Having discussed the predicted ELF/VLF magnitudes in great depth, we now proceed to consider the theoretical predictions for the ELF/VLF harmonic ratio.

4.3. ELF/VLF Harmonic Ratio

[41] As described earlier in this paper, the ELF/VLF harmonic ratio cancels frequency-dependent propagation effects to first order. The second-order effect depends on the spatial distribution of the source currents that generate the first and second harmonics. We now consider the spatial distribution of the second harmonic components of the Hall and Pedersen currents for comparison with the first harmonic components, shown in Figures 10 and 11. The

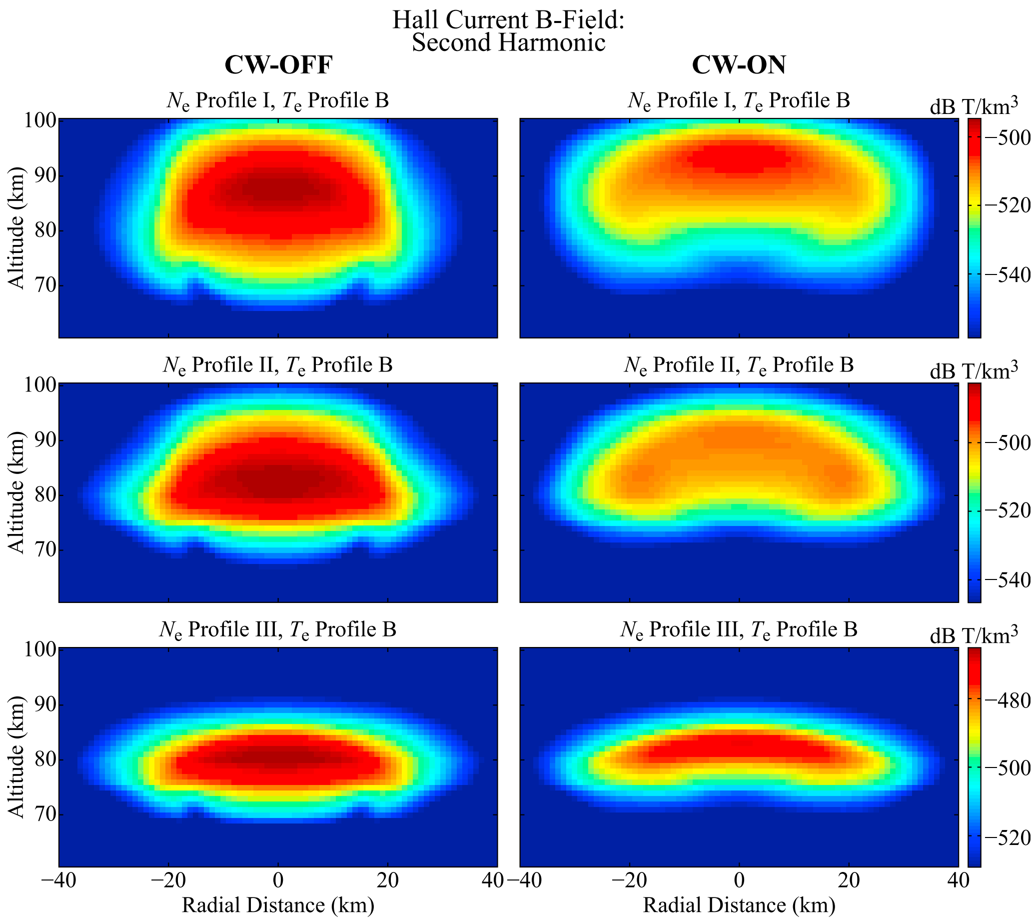

Figure 15. Numerical predictions. Second harmonic (2430 Hz) Hall current *B* field amplitudes as a function of source location. CW-ON and CW-OFF periods are shown as a function of electron density profile.

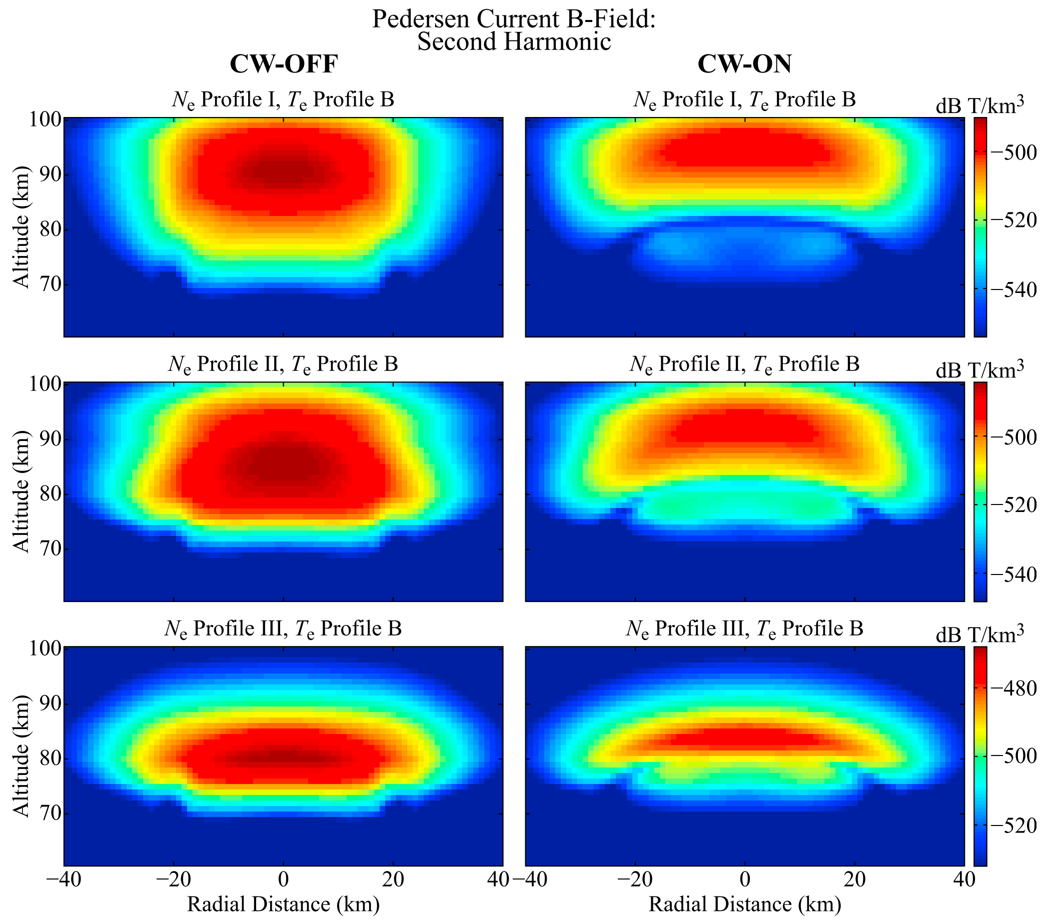

Figure 16. Numerical predictions. Second harmonic (2430 Hz) Pedersen current *B* field amplitudes as a function of source location. CW-ON and CW-OFF periods are shown as a function of electron density profile.

spatial distribution of the *B* fields associated with the second harmonic of the Hall and Pedersen currents are shown in Figures 15 and 16. We point out that during CW-OFF periods, the spatial distribution of the second harmonic of the Hall *B* field is very similar to that of the first harmonic, although the second harmonic of the Pedersen *B* field is somewhat lower in altitude than the first harmonic. During CW-ON periods, however, the second harmonic of the Hall *B* field is "pushed" higher in altitude than the first harmonic, whereas the spatial distribution of the second harmonic of the Pedersen *B* field is very similar to that of the first harmonic. It is thus the case that during both CW-ON and CW-OFF periods, there is at least one major component of the ELF/VLF magnitudes that has a very similar spatial distribution for both the first and second harmonic, indicating that the ELF/VLF harmonic ratio naturally minimizes second-order effects as well as first-order effects. Figures 15 and 16 demonstrate that this is the case for a variety electron density profiles.

[42] Figure 17 (top) shows the ELF/VLF harmonic ratio as a function of electron density profile and electron temperature profile during CW-OFF periods, and Figure 17 (bottom) shows the dB change in harmonic ratio between CW-ON and CW-OFF periods. The negative changes shown in Figure 17 (bottom) indicate that the harmonic ratio is modeled to be higher during CW-ON periods than during CW-OFF periods, consistent with observations. Several combinations of electron density profiles and electron temperature profiles match our observations, both in terms of the CW-OFF harmonic ratio (−16.6 to −19.0 dB) and in terms of the change in harmonic ratio between CW-ON and CW-OFF periods (−2.0 to 5.5 dB): electron density Profiles II and III, together with electron temperature Profiles C and D. The harmonic ratios calculated using these profiles span our observations better than the calculated ELF/VLF magnitudes. We attribute the closeness of this match to the effective cancellation of both first- and second-order propagation effects, which were not conveniently canceled by other measurement techniques. Interestingly, model results (not shown) indicate that the ELF/VLF harmonic ratio is a relatively stable value in terms of observation location, varying by less than ~1 dB within 100 km of the HAARP transmitter.

[43] The harmonic ratio is very sensitive to both the electron density profile and the electron temperature profile used, varying by several dB in both cases. The change in harmonic amplitude at CW-ON/CW-OFF boundaries is also easily detectable and quick to evaluate (only two ELF/VLF frequencies needed). It thus appears that the ELF/VLF harmonic ratio is ideally suited to evaluate HAARP-induced

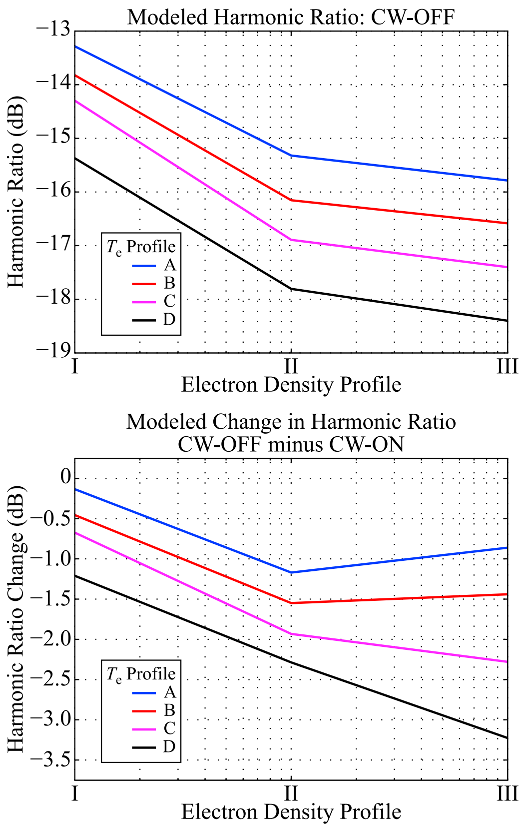

Figure 17. (top) ELF/VLF harmonic ratio (as described in the text) as a function of electron density profile and electron temperature profile. (bottom) The change in ELF/VLF harmonic ratio from CW-OFF to CW-ON conditions.

electron density changes at the altitude of wave generation. Figure 17 (bottom) indicates that (for Profile D) a factor of 2 increase in electron density would result in an additional ~0.25 dB change in the harmonic ratio between CW-ON and CW-OFF periods. In the observations from the current experiment this is not observable above the noise. We can limit the maximum change in electron density to a factor of ~5, based on the ±0.7 dB uncertainty of the measurement, however. The relatively weak ELF/VLF wave generation during the experiment, however, indicates that future experiments may have more success applying this technique to further limit the possible heater-induced change in the electron density with time.

[44] Here we point out that electron density Profiles II and III, together with electron temperature Profiles C and D have most closely matched the change in ELF/VLF magnitudes at CW-ON/CW-OFF boundaries and they also closely reproduce changes in ELF/VLF harmonic ratios that very closely match the observations presented earlier in this paper. Although we have not presented an exhaustive set of electron density and temperature profiles, it is reasonable to conclude that some combination of electron temperature Profiles C and D and some combination of electron density Profiles II and III are reasonable estimates of the physical properties of the *D* region ionosphere during the presented experiment.

[45] Having now discussed the numerical modeling results for both the ELF/VLF wave magnitude and the ELF/VLF harmonic ratio, we continue by addressing the numerical modeling of the ELF/VLF power law exponent.

4.4. ELF/VLF Power Law Exponent

[46] The EPLE values as a function of electron density and electron temperature are shown in Figure 18 (top and middle). Two important results are immediately evident from Figure 18. For the high HF power levels for which these results were calculated, the EPLE decreases significantly as the electron density varies from Profile I to Profile III (i.e., as the electron density increases). This result stands in stark contrast to the simulation results for the ELF/VLF magnitude, which increases sharply between Profiles I and III. Together, these simulation results support the conclusion

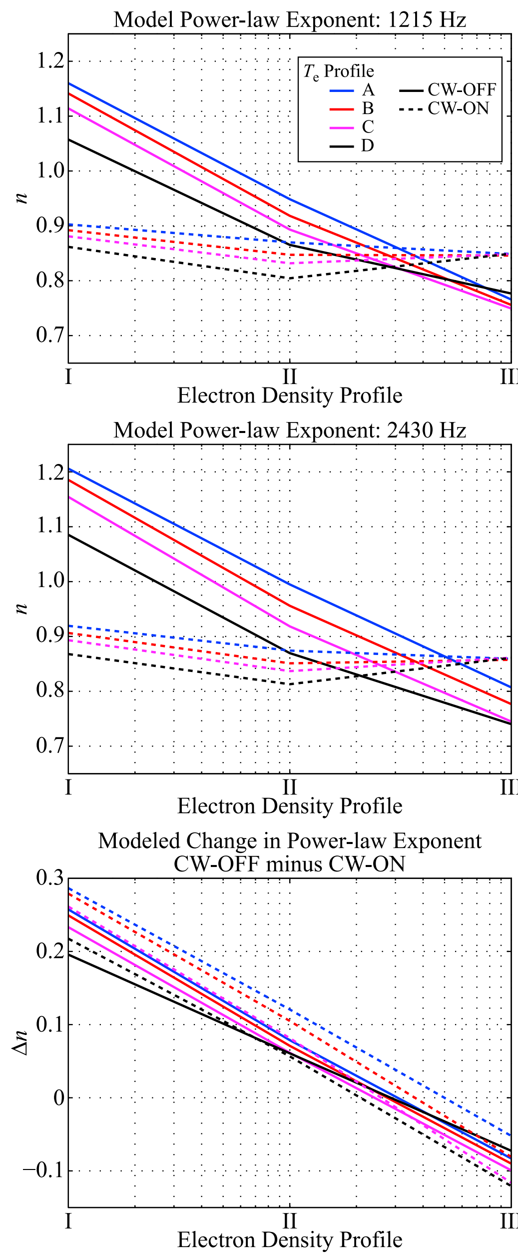

Figure 18. Numerical predictions. (top and middle) Values of n at 1215 and 2430 Hz. (bottom) The change in n from CW-OFF to CW-ON conditions.

that the EPLE does not represent the overall efficiency of ELF/VLF wave generation. A second result that is clearly depicted in Figure 18 is the tempering effect of additional CW heating on the EPLE. Although the EPLE varies significantly as a function of electron density profile under CW-OFF conditions, it is relatively constant under CW-ON conditions. This effect yields the general result that the EPLE may be either higher or lower during CW-ON or CW-OFF periods, depending on the electron density profile and the electron temperature profile employed.

[47] Further conclusions may be drawn by closely inspecting the dependence of EPLE on electron density and electron temperature. A factor of two increase in electron density at 80 km altitude would decrease n by approximately 0.05–0.07. *Milikh and Papadopoulos* [2007] predict this change may occur with a time scale on the order of 1 min (although at ~85 km altitude). The level of noise in our experimental observations of EPLE, however, is much too large to detect this small modification. The ELF/VLF harmonic ratio clearly constitutes a much better measurement for providing limits for possible changes in electron density. The electron temperature is also an important factor in determining the EPLE. Similar to the dependence on electron density, n typically decreases as the electron temperature decreases, despite the indication that the total ELF/VLF magnitude tends to increase with decreasing electron temperature.

[48] The large uncertainty in our experimentally observed EPLEs makes our observations consistent with almost all of our modeling runs. While the ELF/VLF magnitude and the ELF/VLF harmonic ratio appear to be sensitive to ionospheric changes even under low SNR conditions, the EPLE derived from low SNR observations is clearly not a good indicator for ionospheric modification.

5. Discussion and Summary

[49] We have presented experimental evidence indicating that the magnitudes of ELF/VLF waves observed on the ground are significantly reduced when generated together with a broader CW heating beam, and we introduced a new dual-beam HF heating model that similarly reproduced these results. We demonstrated that the ELF/VLF harmonic ratio is also very sensitive to the presence of the CW heating beam and that numerical predictions of the harmonic ratio closely simulated the observed effects. Last, the ELF/VLF power law exponent was shown to be too sensitive to SNR to provide accurate experimental observations relating to ionospheric modification. While the immediate effects of CW heating were apparent in our data set, no significant variations resulting from long-term CW heating were observed. It is possible that long-term heating effects were obscured by noise, however, and theoretical modeling was used to limit the possible long-term electron density changes to a factor of approximately 5 at 80 km altitude.

[50] **Acknowledgments.** This work is supported by ONR grant N000141010909 to the University of Florida. This project is also supported by BAE Systems contract 709372 to the University of Florida. We thank the Polar Aeronomy and Radio Science (PARS) Summer School, which enabled the performance of this experiment.

[51] Robert Lysak thanks reviewers Morris Cohen and Björn Gustavsson for their assistance in evaluating this paper.

References

Banks, P. (1966), Collision frequencies and energy transfer: Electrons, *Planet. Space Sci.*, *14*, 1085–1103.

Banks, P. M., and J. R. Doupnik (1975), A review of auroral zone electrodynamics deduced from incoherent scatter radar observations, *J. Atmos. Terr. Phys.*, *37*, 951–972.

Barr, R., and P. Stubbe (1984), ELF and VLF radiation from the "polar electrojet antenna," *Radio Sci.*, *19*, 1111–1122.

Barr, R., and P. Stubbe (1991), ELF radiation from the Tromsø "Super Heater" facility, *Geophys. Res. Lett.*, *18*, 1035–1038.

Barr, R., and P. Stubbe (1993), ELF harmonic radiation from the Tromsø heating facility, *Geophys. Res. Lett.*, *20*, 2243–2246.

Barr, R., P. Stubbe, and H. Kopka (1991), Long-range detection of VLF radiation produced by heating the auroral electrojet, *Radio Sci.*, *26*, 871–879.

Cohen, M. B., U. S. Inan, M. Gołkowski, and M. J. McCarrick (2010), ELF/VLF wave generation via ionospheric HF heating: Experimental comparison of amplitude modulation, beam painting, and geometric modulation, *J. Geophys. Res.*, *115*, A02302, doi:10.1029/2009JA014410.

Dalgarno, A., M. B. McElroy, M. H. Rees, and J. C. G. Walker (1968), The effect of oxygen cooling on ionospheric electron temperatures, *Planet. Space Sci.*, *16*, 1371–1380.

Getmantsev, C. G., N. A. Zuikov, D. S. Kotik, L. F. Mironenko, N. A. Mityakov, V. O. Rapoport, Y. A. Sazonov, V. Y. Trakhtengerts, and V. Y. Eidman (1974), Combination frequencies in the interaction between high-power short-wave radiation and ionospheric plasma, *Sov. Phys. JETP, Engl. Transl.*, *20*, 101–102.

Huxley, L. G. H., and J. A. Ratcliffe (1949), A survey of ionospheric cross-modulation, *Proc. Inst. Electr. Eng.*, *96*, 433–440.

Janches, D., D. C. Fritts, M. J. Nicolls, and C. J. Heinselman (2009), Observations of *D*-region structure and atmospheric tides with PFISR during active aurora, *J. Atmos. Sol. Terr. Phys.*, *71*, 688–696, doi:10.1016/j.jastp.2008.08.015.

Lehtinen, N. G., and U. S. Inan (2008), Radiation of ELF/VLF waves by harmonically varying currents into a stratified ionosphere with application to radiation by a modulated electrojet, *J. Geophys. Res.*, *113*, A06301, doi:10.1029/2007JA012911.

Maslin, N. M. (1974), Theory of energy flux and polarization changes of a radio wave with two magnetoionic components undergoing self demodulation in the ionosphere, *Proc. R. Soc. London, Ser. A*, *341*, 361–381.

Mentzoni, M. H., and R. V. Row (1963), Rotational excitation and electron relaxation in nitrogen, *Phys. Rev.*, *130*, 2312–2316.

Milikh, G. M., and K. Papadopoulos (2007), Enhanced ionospheric ELF/VLF generation efficiency by multiple timescale modulated heating, *Geophys. Res. Lett.*, *34*, L20804, doi:10.1029/2007GL031518.

Moore, R. C. (2007), ELF/VLF wave generation by modulated HF heating of the auroral electrojet, Ph.D. thesis, Stanford Univ., Stanford, Calif.

Moore, R. C., U. S. Inan, and T. F. Bell (2006), Observations of amplitude saturation in ELF/VLF wave generation by modulated HF heating of the auroral electrojet, *Geophys. Res. Lett.*, *33*, L12106, doi:10.1029/2006GL025934.

Moore, R. C., U. S. Inan, T. F. Bell, and E. J. Kennedy (2007), ELF waves generated by modulated HF heating of the auroral electrojet and observed at a ground distance of 4400 km, *J. Geophys. Res.*, *112*, A05309, doi:10.1029/2006JA012063.

Papadopoulos, K., C. L. Chang, P. Vitello, and A. Drobot (1990), On the efficiency of ionospheric ELF generation, *Radio Sci.*, *25*, 1311–1320.

Papadopoulos, K., T. Wallace, M. McCarrick, G. M. Milikh, and X. Yang (2003), On the efficiency of ELF/VLF generation using HF heating of the auroral electrojet, *Plasma Phys. Rep.*, *29*, 561–565.

Papadopoulos, K., T. Wallace, G. M. Milikh, W. Peter, and M. McCarrick (2005), The magnetic response of the ionosphere to pulsed HF heating, *Geophys. Res. Lett.*, *32*, L13101, doi:10.1029/2005GL023185.

Payne, J. A. (2007), Spatial structure of very low frequency modulated ionospheric currents, Ph.D. thesis, Stanford Univ., Stanford, Calif.

Payne, J. A., U. S. Inan, F. R. Foust, T. W. Chevalier, and T. F. Bell (2007), HF modulated ionospheric currents, *Geophys. Res. Lett.*, *34*, L23101, doi:10.1029/2007GL031724.

Prasad, S. S., and D. R. Furman (1973), Electron cooling by molecular oxygen, *J. Geophys. Res.*, *78*, 6701–6707.

Rietveld, M. T., H. Kopka, and P. Stubbe (1986), *D*-region characteristics deduced from pulsed ionospheric heating under auroral electrojet conditions, *J. Atmos. Terr. Phys.*, *48*, 311–326.

Rietveld, M. T., P. Stubbe, and H. Kopka (1989), On the frequency dependence of ELF/VLF waves produced by modulated ionospheric heating, *Radio Sci.*, *24*, 270–278.

Rodriguez, J. V. (1994), Modification of the Earth's ionosphere by very-low-frequency transmitters, Ph.D. thesis, Stanford Univ., Stanford, Calif.

Stubbe, P., and H. Kopka (1977), Modulation of polar electrojet by powerful HF waves, *J. Geophys. Res.*, *82*, 2319–2325.

Stubbe, P., and W. S. Varnum (1972), Electron energy transfer rates in the ionosphere, *Planet. Space Sci.*, *20*, 1121–1126.

Stubbe, P., H. Kopka, M. T. Rietveld, and R. L. Dowden (1982), ELF and VLF generation by modulated HF heating of the current carrying lower ionosphere, *J. Atmos. Terr. Phys.*, *44*, 1123–1135.

Tomko, A. A. (1981), Nonlinear phenomena arising from radio wave heating of the lower ionosphere, *Tech. Rep. PSU-IRL-SCI-470*, Ionos. Res. Lab., Pa. State Univ., University Park, Pa.

Tomko, A. A., A. J. Ferraro, and H. S. Lee (1980), *D* region absorption effects during high-power radio wave heating, *Radio Sci.*, *15*, 675–682.

Villaseñor, J., A. Y. Wong, B. Song, J. Pau, M. McCarrick, and D. Sentman (1996), Comparison of ELF/VLF generation modes in the ionosphere by the HIPAS heater array, *Radio Sci.*, *31*, 211–226.

D. Agrawal and R. C. Moore, Department of Electrical and Computer Engineering, University of Florida, PO Box 116200, 319 Benton Hall, Gainesville, FL 32611, USA. (moore@ece.ufl.edu)